Modulation of Electronic Properties in Neutral and Oxidized Oligothiophenes Substituted with Conjugated Polyaromatic Hydrocarbons

Tracey M. Clarke,[†] Keith C. Gordon,*[,†] Pawel Wagner,[‡] and David L. Officer[‡]

Department of Chemistry and MacDiarmid Institute for Advanced Materials and Nanotechnology, University of Otago, P.O. Box 56, Dunedin, New Zealand, and Nanomaterials Research Centre and MacDiarmid Institute for Advanced Materials and Nanotechnology, Massey University, Private Bag 11222, Palmerston North, New Zealand

Received: October 22, 2006; In Final Form: January 23, 2007

The structural and electronic properties of neutral and oxidized terthiophenes substituted with polyaromatic systems have been investigated using a combination of both Raman and electronic absorption spectroscopy in conjunction with density functional theory calculations. Naphthylethenyl terthiophene exhibits structural and electronic properties, in both the neutral and oxidized species, that are dominated by the terthiophene backbone, in a manner similar to that previously reported for phenylethenylterthiophene. Anthracenylethenyl terthiophene, on the other hand, displays properties that are dominated by the anthracene group. Unlike both phenylethenyl and naphthylethenyl terthiophene, which have electronic absorption spectra dominated by transitions between molecular orbitals that are delocalized throughout the molecules, the absorption spectrum of anthracenylethenyl terthiophene consists of a simple addition of the absorption bands of the separate terthiophene and anthracenylethene chromophores. This is the result of a spatial partitioning of its molecular orbitals that effectively electronically decouples the anthracene and terthiophene moieties. Upon oxidation, the naphthylethenylterthiophene σ-dimerizes to form sexithiophene charged species and spectral signatures of the sexithiophene backbone are evident in both the electronic absorption and resonance Raman spectra. In contrast, these signatures are absent in the corresponding spectra of the oxidized anthracenylethenylterthiophene, suggesting that the anthracene group is the primary site of the structural changes induced by oxidation.

I. Introduction

In recent years, oligothiophenes have received considerable attention due to their potential application in organic electronic devices such as OLEDs[1,2] and FETs.[3,4] Although it was π-conjugated polymers that provided the initial point of interest in this field, their general intractability means that they are difficult to process for such applications. In contrast, oligothiophenes are soluble while still retaining the desirable semiconductive properties of the corresponding polymer and thus have significant potential for organic electronics. Indeed, unsubstituted sexithiophene and octithiophene are both reported to be highly efficient materials for FET devices.[5−8] However, the effect of substitution on the structural and electronic properties of oligothiophenes and its consequent influence on device efficiency remains largely unexplored. A number of methods exist for ascertaining such properties. The structural properties of oligothiophenes have been studied by Raman spectroscopy,[9−12] which is sensitive to effective conjugation length and the structural changes that occur upon oxidation. This latter phenomenon is of particular interest because it is often the oxidized/doped species (the polaron or bipolaron) that is the active charge carrier in electronic devices. Raman studies on these oligothiophene charged species have shown the expected development of a quinoidal bond structure along the thiophene backbone upon oxidation.[13−16] The transition from an aromatic to quinoid bond sequence is manifested as downshifts of the thiophene C═C stretching modes. The Raman spectra of unsubstituted sexithiophene before and after oxidation, for example, show that the most intense band in the spectrum, a symmetrical thiophene C═C stretching mode, downshifts from 1459 to 1440 cm^{-1} as the radical cation is created.[17]

Investigations into oligothiophene structure have been aided significantly through the use of computational chemistry. Semiempirical,[18,19] ab initio,[20−24] and density functional theory (DFT)[25−29] techniques have been extensively applied to oligothiophenes and their charged species to model their structural and spectroscopic properties. These are particularly powerful methods when used in conjunction with experimental vibrational spectroscopy, allowing comparison between measured and predicted spectra. A good correlation between these indicates that the calculated geometry is a reliable representation of the true structure; as such, important information such as molecular orbitals and spin densities can be derived from the calculated data.[30] Early low-level calculations on oligothiophene polarons and bipolarons indicated the formation of quinoid-type bond sequences within the defects,[31−33] and the later use of higher levels of theory substantiated this finding.[13,34,35] These studies also investigated the spatial extent of the defects, and the calculated spectra that result from them. Such investigations have demonstrated that oligothiophene polarons extend over approximately three or four[14] thiophene rings whereas bipolarons extend over six[36] to nine[32,37] rings (depending on the definition of the defect boundaries).

Electronic absorption spectroscopy is also an important technique for the investigation of both neutral oligothiophenes[37−40]

* Corresponding author. Fax: (+64) 3 479 7906. E-mail: kgordon@alkali.otago.ac.nz.
[†] University of Otago.
[‡] Massey University.

10.1021/jp066922r CCC: $37.00
Published on Web 03/07/2007

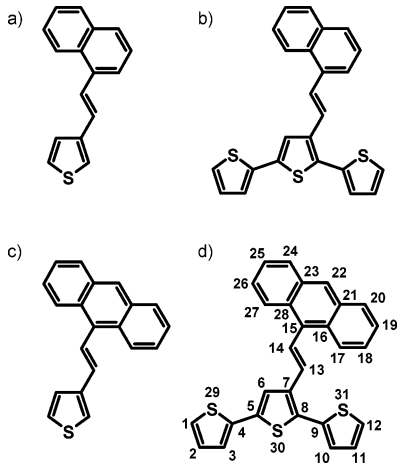

Figure 1. Structures of naph-e-1T (a), naph-e-3T (b), anth-e-1T (c), and anth-e-3T (d). The atom labeling system is shown for anth-e-3T, where ϕ_1 = (S29,C4,C5,S30), ϕ_2 = (S30,C8,C9,S31), ϕ_3 = (C6,C7,-C13,C14), and ϕ_4 = (C13,C14,C15,C16).

and their charged species.[41−46] It is a useful method for following oligothiophene oxidation reactions and characterizing the nature of the end products. However, it can be difficult to measure the absorption spectra of the radical cations of short unsubstituted oligothiophenes due to their high reactivity and short lifetimes. The terthiophene radical cation, for instance, has a lifetime on the microsecond time scale[43,47,48] and rapidly σ-dimerizes to form sexithiophene.[44,49] Sexithiophene radical cations are significantly more stable than their terthiophene counterparts[49] and sexithiophene dications are often observed if the oxidation reaction is continued.

The absorption spectra of the neutral oligothiophenes can also offer an insight into their electronic properties, especially when used in conjunction with time-dependent DFT (TD-DFT) calculations.[25,50−52] These calculations provide a variety of information about each excited state: vertical transition energies, oscillator strengths, and the molecular orbitals involved in the excitation/s comprising the transition, for example. Care must be taken in the application of such results to experimental data as TD-DFT calculations are known to often show large deviations between experimental and calculated transition energies of between 0.4 and 0.7 eV for the neutral and charged species of conjugated systems.[52,53] However, the predicted intensity patterns and relative band separations are often consistent with the measured spectra, thereby allowing the calculated electronic properties to be used in interpreting the observed properties of the compounds.

The two molecules examined here are terthiophenes substituted in the 3′ position with polyaromatic hydrocarbons (naphthalene or anthracene), the two moieties being connected by an ethenyl linkage. These compounds, termed naph-e-3T and anth-e-3T (Figure 1), have the potential to provide a combination of the semiconductive properties of oligothiophenes with the emissive qualities of large aromatic systems. The purpose of this work is to investigate the structural and electronic properties of both the neutral and oxidized forms of these aryl-substituted terthiophenes using both Raman and electronic absorption spectroscopy in conjunction with DFT calculations and cyclic voltammetry. Because of the σ-dimerization that occurs upon oxidation of non end-capped terthiophenes (such as those studied here), it is also necessary to perform calculations on the corresponding head-to-head substituted sexithiophenes. In addition, the thiophene-based analogues (naph-e-1T and anth-e-1T; Figure 1) have proven useful for comparison on the effect of differing substitutents as has the previously studied[54−56] styryl-substituted terthiophene phenyl-e-3T.

II. Experimental Section

A. Materials and General Synthetic Procedures. AR grade solvents and reagents were used for synthesis and were obtained from commercial sources. Dry THF was prepared by passing argon-degassed solvent through activated alumina columns. 3-(2-Naphthalen-1-yl)thiophene was synthesized according to a literature procedure.[57]

B. Analytical Measurements. NMR spectra were recorded at 400.13 MHz (^{1}H) and 100.1 MHz (^{13}C) using a Brüker 400 Avance spectrometer running X-WIN-NMR software. The chemical shifts are relative either to tetramethylsilane (TMS) or to the residual proton signal in deuterated solvents ($CDCl_3$ δ 7.27). ^{13}C NMR shifts are relative to $CDCl_3$ (δ 77.0). Chemical shifts are reported as position (δ), multiplicity (s = singlet, d = doublet, t = triplet, q = quartet, dd = doublet of doublets, m = multiplet), relative integral, coupling constant (J in Hz), and assignment. High-resolution mass spectrometry (HRMS) and fast-atom bombardment (FAB) and electron ionization (EI) mass spectrometry were carried out using a Varian VG70-250S double-focusing magnetic-sector mass spectrometer. Samples analyzed by FAB-HRMS were supported on an *m*-nitrobenzyl alcohol matrix. The data was put through a MASSPEC II data system to give ±5 ppm error formulations on molecular ions. Major fragmentations are given as percentages relative to the base-peak intensity. Melting points are uncorrected.

Cyclic voltammograms were measured at room temperature using 5×10^{-4} mol L^{-1} oligothiophene solutions. All solutions were prepared in 0.1 mol L^{-1} tetrabutylammonium perchlorate (TBAP) in acetonitrile and degassed with nitrogen for 5 min prior to measurement. The data were acquired at scan speeds of 0.2−2.0 V s^{-1} using an AdInstruments Powerlab 4sp potentiostat controlled by a PC running Powerlab EChem software. The electrochemical cell consisted of a 1.0 mm diameter platinum working electrode embedded in a Kel-F cylinder with a platinum auxiliary electrode and an Ag/AgCl reference electrode. The decamethylferrocenium/decamethylferrocene ($Me_{10}Fc^{+/0}$) redox couple was used as an internal standard.[58]

FT-Raman spectra of the neutral terthiophenes were recorded from solid powder samples using a Bruker IFS-55 FT-interferometer bench equipped with an FRA/106 Raman accessory and an InGaAs D425 or liquid nitrogen cooled Ge D418-T Raman detector. Radiation of 1064 nm from an Nd:YAG laser with an operating power of 100 mW was utilized for Raman excitation. The FT-Raman spectra were collected after an average of 64 scans at a resolution of 4 cm^{-1}.

Resonance Raman spectra of the oxidized films and acetonitrile solutions were measured with an excitation wavelength of 752 nm using a system described previously,[30] except that a 50 μm entrance slit to the spectrograph was used. The neutral films were measured using 413 nm excitation.

Electronic absorption spectra of the neutral compounds were measured in spectrophotometric grade acetonitrile and dichloromethane at room temperature (1×10^{-5} mol L^{-1}) from 200 to 800 nm on a Varian Cary 500 Scan UV−vis−NIR Spectrophotometer using Cary WinUV Scan Application software. Spectra were also measured of the oxidized solutions at each stage of the oxidation process from 200 to 2000 nm.

C. Computational Methods. Density functional theory (DFT) calculations were carried out using the Gaussian 03

program[59] with the B3LYP method in conjunction with the 6-31G(d) basis set. Geometry optimizations of the neutral oligothiophenes and their radical cations and dications were performed with the thiophene rings in an all-anti−gauche configuration and the ethenyl moiety connected to the central thiophene ring at an acute dihedral angle. The geometry optimizations were performed with no constraints on planarity. However, in the case of the head-to-head sexithiophenes, it was required that C_2 symmetry be imposed onto these systems due to the large number of basis functions involved in the calculation. Even so, the 3-21G(d) basis set had to be used for the largest molecule (anth-e-3T)$_2$ and its charged species. All radical cation calculations were performed using the spin-unrestricted wavefunction (UB3LYP). The geometry optimizations were followed by a frequency calculation for each species of the vibrational frequencies and corresponding IR and Raman intensities. A scale factor of 0.961 was applied to the B3LYP/6-31G(d) predicted frequencies, as previously recommended.[60] However, no standard scale factor for B3LYP/3-21G(d) could be found in the literature. To provide a fair comparison between the two basis sets, the scale factor for B3LYP/3-21G(d) was chosen such that the highest energy vibrational mode in the region of interest (500−1650 cm^{-1}), the ethenyl stretching mode ν(C═C)$_{ethenyl}$, was at an equivalent frequency for both basis sets. The 3-21G(d) scale factor has therefore been calculated at 0.970. Vertical electronic excitation energies were also calculated for the neutral oligothiophenes and their respective radical cations and dications using time-dependent density functional theory (TD-DFT) on the optimized geometries.

D. Oxidation Methods. Solid films of the oxidized sexithiophenes were produced electrochemically on ITO glass immersed in an oligothiophene solution by applying an oxidizing potential (0.9−1.2 V) for deposition times of 2−10 min. The auxiliary electrode was a 1 cm^3 platinum mesh and an Ag/AgCl reference electrode was used. Films of the neutral sexithiophenes were generated from the terthiophenes by applying a reducing potential of 0 V after the initial oxidation deposition.

Chemical oxidations were performed using 1.0×10^{-5} and 1.0×10^{-4} mol L^{-1} oligothiophene solutions, prepared with spectrophotometric grade acetonitrile. Aliquots (5−20 μL) of oxidant, a solution of 8×10^{-4} mol L^{-1} copper perchlorate in acetonitrile ($Cu(ClO_4)_2/CH_3CN$), were added until the desired charged species formed. Reduction of each final oxidation product was achieved by adding one drop of a 2% hydrazine aqueous solution.

E. Synthesis. *(1) 3-(2-Anthracen-9-ylethenyl)thiophene (anth-e-1T).* 3-Thiophenecarboxaldehyde (448 mg, 4×10^{-3} mol) and 9-anthracenylmethyltriphenylphosphonium bromide[61] (2.34 g, 1.1 equiv) were dissolved in THF (20 mL), and DBU was added (3.04 g, 0.02 mol) and the resulting mixture refluxed overnight under argon. The reaction mixture was filtered, diluted with dichloromethane (50 mL), and washed with dilute hydrochloric acid. The organic layer was separated out, dried over magnesium sulfate, and evaporated to dryness under vacuum at 50 °C. The resulting crude solid was recrystallized from ethanol to give 630 mg of fine gold-like plates of anth-e-1T (55%), mp 139−141 °C. ^{1}H NMR (400 MHz): δ 8.37 (s, 1H, Anth-H10), 8.35−8.32 (m, 2H, Anth-H1, H8), 8.00−7.97 (m, 2H, Anth-H5, H6), 7.73 (d, 1H, J = 16.4 Hz, vinyl-H), 7.55 (d, 1H, J = 4.8 Hz, Th-H4), 7.76−7.44 (m, 4H, Anth-H2, H3, H6, H7), 7.41 (dd, 1H, J = 4.8 and 2.4 Hz, Th-H5), 7.33 (d, 1H, J = 2.4 Hz, Th-H2), 6.93 (d, 1H, J = 16.4 Hz, vinyl-H). Assignments aided by COSY. ^{13}C NMR (100 MHz): δ 140.1, 132.6, 131.4, 129.6, 128.6, 126.43, 126.38, 126.0, 125.4, 125.1, 124.9, 124.6, 122.8. MS M$^+$ (EI, *m*/*z*, %): 286 (100), 285 (49), 253 (29), 252 (27), 202 (28). HRMS: 286.08167 (expected for $C_{20}H_{14}S$ 286.08162).

(2) 3′-(2-Naphthalen-1-ylvinyl)[2,2′;5′,2″]terthiophene (naph-e-3T). 1-Naphthalenecarboxaldehyde (312 mg, 2×10^{-3} mol) and diethyl [2,2′;5′,2″]terthiophen-3′-ylmethylphosphonate[62] (840 mg, 1.1 equiv) were dissolved in THF (20 mL), and potassium *tert*-butoxide (246 mg, 1.1 equiv) was added. The resulting mixture was stirred at room temperature overnight. The reaction mixture was diluted with chloroform (100 mL) and washed with diluted hydrochloric acid and water. The organic layer was separated out, dried over magnesium sulfate, and evaporated to dryness under vacuum at 60 °C. The resulting crude solid was recrystallized from ethanol to give naph-e-3T as yellow needles (326 mg, 69%), mp 118−120 °C. ^{1}H NMR (400 MHz): δ 8.23 (d, 1H, J = 8.8 Hz, Napht-H8), 7.91−7.80 (m, 2H, Napht-H5, H2), 7.81 (d, 1H, J = 16.0 Hz, vinyl-H), 7.70 (d, 1H, J = 7.2 Hz, Napht-H3), 7.59−7.46 (m, 3H, Napht-H4, H6, H7), 7.54 (s, 1H, TTh-H4′H), 7.38 (d, 1H, J = 16.0 Hz, vinyl-H), 7.36 (dd, 1H, J = 1.2 and 5.2 Hz, Tth-H5″), 7.27 (dd, 1H, J = 1.2 and 5.2 Hz, Tth-H5), 7.24 (dd, 1H, J = 1.2 and 3.6 Hz, Tth-H3″), 7.20 (dd, 1H, J = 1.2 and 3.6 Hz, Tth-H3), 7.10 (dd, 1H, J = 3.6 and 5.2 Hz, Tth-H4″), 7.05 (dd, 1H, J = 3.6 and 5.2 Hz, Tth-H4). Assignments aided by COSY. ^{13}C NMR (100 MHz): δ 136.70, 136.66, 136.1, 135.1, 134.8, 133.7, 131.7, 131.9, 131.2, 128.6, 128.0, 127.9, 127.8, 127.3, 127.1, 126.4, 126.1, 125.9, 125.7, 124.9, 124.5, 124.2, 123.7, 123.6, 122.4. MS M$^+$ (EI, *m*/*z*, %): 400 (100), 399 (11), 367 (10), 273 (11). HRMS: 400.04119 (expected for $C_{24}H_{16}S_3$ 400.04142).

(3) 3′-(2-Anthracen-9-yl-vinyl)[2,2′;5′,2″]terthiophene (anth-e-3T). 9-Anthracenecarboxaldehyde (412 mg, 2×10^{-3} mol) and diethyl [2,2′;5′,2″]terthiophen-3′-ylmethylphosphonate[62] (840 mg, 1.1 equiv) were dissolved in THF (20 mL), and potassium *tert*-butoxide (1.1 equiv for reaction center) was added. The resulting mixture was stirred at room temperature overnight. The reaction mixture was diluted with chloroform (100 mL) and washed with diluted hydrochloric acid and water. The organic layer was separated out, dried over magnesium sulfate, and evaporated to dryness under vacuum at 60 °C. The resulting crude solid was recrystallized from ethanol to give anth-e-3T as yellow needles (720 mg, 80%), mp 196−197 °C. ^{1}H NMR (400 MHz): δ 8.39 (s, 1H, Anth-H10), 8.38−8.35 (m, 2H, Anth-H1, H8), 8.03−7.98 (m, 2H, Anth-H4, H5), 7.85 (d, 1H, J = 16.0 Hz, vinyl-H), 7.70 (s, 1H, Tth-H4′), 7.49−7.46 (m, 4H, Anth-H2, H3, H6, H7), 7.29−7.28 (m, 2H, Tth-H3, H3″), 7.53 (dd, 1H, J = 1.2 and 5.2 Hz, Tth-H″), 7.15 (d, 1H, J = 16.0 Hz, vinyl-H), 7.13 (dd, 1H, J = 1.2 and 5.6 Hz, Tth-H5), 7.06 (dd, 1H, J = 3.6, 5.2 Hz, Tth-H4″), 6.97 (dd, 1H, J = 3.6 and 5.2 Hz, Tth-H4). ^{13}C NMR (100 MHz): δ 136.7, 136.34, 136.28, 134.8, 132.5, 132.0, 131.5, 130.2, 129.6, 128.7, 128.0, 127.7, 127.0, 126.64, 126.57, 126.4, 126.0, 125.5, 125.2, 125.0, 124.3, 122.4. MS M$^+$ (EI, *m*/*z*, %): 450 (100), 449 (10), 417 (18), 202 (11). HRMS: 450.05666 (expected for $C_{28}H_{14}S_3$ 450.05707).

III. Results and Discussion

A. Terthiophene Geometry. The X-ray crystal structure of anth-e-3T has been determined.[63] The calculated geometry of this molecule offers an excellent correspondence with the crystal structure, as shown in Table 1. The mean absolute deviation in the CC bond lengths between the calculated and experimental structures is 0.012 Å. In addition, the crystal structure provides evidence for the low-energy barrier predicted for rotation about ϕ_2:[56] dual occupation of two atom sites by both a carbon and a

TABLE 1: Calculated and Experimental Structural Parameters of anth-e-3T, Derived from DFT (B3LYP/6-31G(d)) and the Crystal Structure, Respectively, Using the Atom Labeling System Shown in Figure 1[a]

	calculated	experimental	Δ (calc − exp)
	bond (Å)		
C1−C2	1.37	1.35	0.02
C2−C3	1.42	1.45	−0.03
C3−C4	1.38	1.42	−0.04
C4−C5	1.45	1.46	−0.01
C5−C6	1.37	1.36	0.01
C6−C7	1.43	1.43	0.00
C7−C8	1.39	1.38	0.01
C8−C9	1.45	1.46	−0.01
C9−C10	1.38	1.34/1.38	0.04/0.00
C10−C11	1.42	1.62/1.44	0.20/0.02
C11−C12	1.37	1.32	0.05
C7−C13	1.46	1.46	0.00
C13−C14	1.35	1.33	0.02
C14−C15	1.48	1.48	0.00
C15−C16	1.42	1.41	0.01
C15−C28	1.42	1.41	0.01
C16−C17	1.43	1.42	0.01
C16−C21	1.44	1.44	0.00
C17−C18	1.37	1.36	0.01
C18−C19	1.42	1.42	0.00
C19−C20	1.42	1.35	0.07
C20−C21	1.43	1.41	0.02
C21−C22	1.40	1.39	0.01
C22−C23	1.40	1.40	0.00
C23−C24	1.43	1.42	0.01
C23−C28	1.45	1.44	0.01
C24−C25	1.37	1.35	0.02
C25−C26	1.42	1.41	0.01
C26−C27	1.37	1.35	0.02
C27−C28	1.43	1.43	0.00
	dihedral angle (deg)		
ϕ_1 (S29,C4,C5,S30)	161	167	−6
ϕ_2 (S30,C8,C9,S31)	141	137/43	4/98
ϕ_3 (C6,C7,C13,C14)	22	17	5
ϕ_4 (C13,C14,C15,C16)	51	62	−11

[a] The data for both crystal structure conformers are presented for the applicable parameters (anti/syn).

sulfur atom is evident, indicating the presence of both syn−gauche and anti−gauche conformers in the crystal (this duality is depicted in Figure S1, Supporting Information). For solid state anth-e-3T, the dihedral angle ϕ_2 is either 43° or 137°. The calculated ϕ_2 dihedral angle is anti−gauche (141°). The other thiophene inter-ring dihedral angle, ϕ_1, is well predicted by the calculation (161°), with a deviation from the crystal structure data of only 6°.

The crystal structure of anth-e-3T shows the anthracene substituent to be severely twisted in relation to the terthiophene backbone with a ϕ_4 angles of 62°. This is clearly a result of the steric interaction between the bulky anthracenyl group and the rest of the molecule: the crystal structure of a cyanostyryl substituted terthiophene,[63] which has only a phenyl substituent, has a significantly smaller ϕ_4 dihedral angle (9°). The calculated values of ϕ_4 for anth-e-3T and 4-cyanostyrylterthiophene are respectively 51° and 5°; i.e., the calculation underestimates ϕ_4 for both compounds.

B. Sexithiophene Geometry. The calculated (B3LYP/6-31G(d)) structures of (naph-e-3T)$_2$ (the head-to-head sexithiophene with 3′ and 3′′′′ naphthylethenyl substituents) and its charged species are displayed in a bond length alternation diagram, as shown in Figure S2a,b, which show that a quinoidal bond structure forms in the center of the sexithiophene backbone upon removal of an electron/s, while the terminal rings retain their aromaticity. However, in contrast to the evenly distributed bond lengths predicted for the unsubstituted sexithiophene charged species,[54] the structural defect of (naph-e-3T)$_2^{\bullet+/2+}$ is localized over a smaller area of the thiophene backbone. The charged defect appears to be confined by the naphthylethenyl substituents: only the *two* central rings are fully quinoidal, in contrast to the *four* quinoidal central rings observed for the unsubstituted sexithiophene radical cation and dication.[54] The confinement of the charged defect in (naph-e-3T)$_2^{\bullet+/2+}$ is very similar to that observed for the styryl-substituted sexithiophene, (phenyl-e-3T)$_2^{\bullet+/2+}$.[54]

The defect confinement along the sexithiophene backbone of (naph-e-3T)$_2^{\bullet+/2+}$ can be observed clearly when the changes in bond length from the neutral species are examined (Figure S2c). The largest changes are present in the area of the sexithiophene backbone between the positions of the naphthylethenyl groups, with the defect confinement being more evident in the dication structure. Within the confined central thiophene region, an average absolute bond length change of 0.046 Å is predicted for (naph-e-3T)$_2^{2+}$ relative to the neutral species. However, considerably smaller bond length changes are calculated for the termini: the average absolute change in bond length for the two terminal thiophene rings of (naph-e-3T)$_2^{2+}$ is 0.013 Å. The bond length changes from the neutral species to the dication are therefore over 3 times greater in the central region of the sexithiophene backbone than in the terminal rings. The ethenyl bonds have an average absolute bond length change of 0.023 Å for the creation of (naph-e-3T)$_2^{2+}$, indicating that the bipolaronic defect preferentially extends into the naphthylethenyl group rather than into the thiophene backbone termini. In turn, this suggests that, relative to (phenyl-e-3T)$_2$,[54] the naphthyl group can stabilize the charged defect.

The sexithiophene (anth-e-3T)$_2$ was too large to perform calculations with the 6-31G(d) basis set, even with the constraint of C_2 symmetry—this was particularly the case for the radical cation, which requires a spin-unrestricted calculation. As such, the smaller 3-21G(d) basis set was used instead. Due to this necessity, a B3LYP/3-21G(d) geometry calculation was also performed on (naph-e-3T)$_2$ and its charged species for comparative purposes.

There is little difference between the (naph-e-3T)$_2$ bond lengths calculated using either the 3-21G(d) or the 6-31G(d) basis sets; and the two sets predict similar structural changes upon oxidation of (naph-e-3T)$_2$. The bond labeling scheme for (naph-e-3T)$_2$ is illustrated in Figure 2a, and the B3LYP/3-21G(d) bond length alternation diagrams are shown in Figure 3a,b. The average deviation in bond length between the two basis sets is 0.002 Å with a maximum deviation of 0.005 Å. Despite this, the 3-21G(d) basis set predicts a slightly greater preference for the sexithiophene backbone as the location for the charged defect rather than the substituents compared to that observed for 6-31G(d). For example, the average absolute change in bond length of the central thiophene rings upon creation of the dication increases from 0.046 Å (6-31G(d)) to 0.049 Å (3-21G(d)) whereas that of the ethenyl group decreases from 0.023 to 0.018 Å. In other words, the 6-31G(d) basis set predicts a more even distribution of structural change across the molecule upon oxidation than does 3-21G(d), for which the charged defect is more strongly localized on the sexithiophene backbone.

The (anth-e-3T)$_2$ charged species (calculated using B3LYP/3-21G(d), as shown in Figure 4; the bond labeling scheme is displayed in Figure 2b) show structural changes that are quite different compared to the corresponding naphthylethenyl-sexithiophenes. The bond length changes along the thiophene backbone are much smaller; for instance, the central thiophene

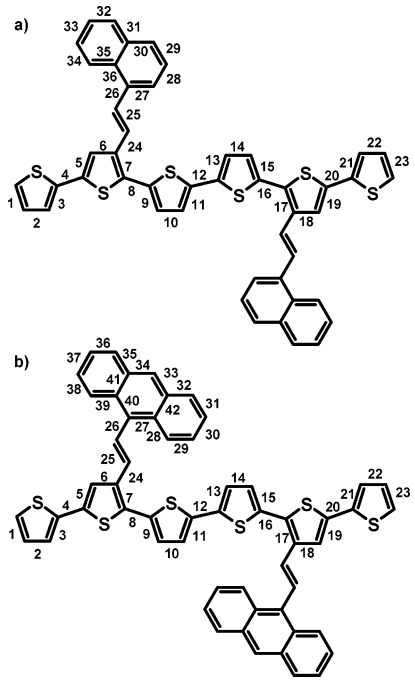

Figure 2. Bond labeling systems for the two head-to-head sexithiophenes (naph-e-3T)$_2$ (a) and (anth-e-3T)$_2$ (b).

region shows an average absolute bond length change of 0.040 Å upon formation of the dication from the neutral molecule. In addition to these smaller thiophene bond length changes, those calculated for the anthracenylethenyl substituents are much larger than that calculated for the naphthylethenyl substituents in (naph-e-3T)$_2$. The ethenyl unit has an average change in bond length of 0.029 Å and although the anthracenyl group has an average change of 0.008 Å, the CC bonds directly attached to the ethenyl moiety lengthen significantly (by 0.019 and 0.022 Å). Indeed, although (anth-e-3T)$_2$ shows the standard defect confinement along the thiophene backbone that is observed for (naph-e-3T)$_2$ and all the styryl sexithiophenes, if the conjugation path is considered to be the "substituent−bithiophene−substituent" path, then the defect confinement is barely evident at all (Figure 4d). Although the majority of the structural change is still located in the center of the sexithiophene backbone, the anthracenyl groups are now dominating the edges of the charged defect and it extends in this direction rather than toward the terminal thiophene rings. This is in contrast to the highly confined defect of (phenyl-e-3T)$_2^{\bullet+/2+}$.[54] It also represents an extension of the partial breakdown of defect confinement that was observed for (naph-e-3T)$_2$ such that the collapse of the confinement is complete.

C. Spin Densities. The geometry calculations also provide spin densities for the terthiophene and sexithiophene radical cations. An examination of these data (Tables S1 and S2) shows that varying the aryl group has a substantial effect on the distribution of spin density in the radical cations. Increasing the size of the aryl group from a phenyl ring to an anthracene group (anth-e-3T$^{\bullet+}$) causes a shift in spin density from the terthiophene unit to the aryl group itself. If the spin densities are summed over each of these sections of the molecule, this trend can be seen more clearly. In the case of phenyl-e-3T$^{\bullet+}$, 80% of the total spin density is localized on the terthiophene backbone. When the aryl group is a naphthalene (naph-e-3T$^{\bullet+}$), this figure drops to 66%. In anth-e-3T$^{\bullet+}$, only 45% of the spin density is situated on the terthiophene—the other 55% is localized on the anthracenylethenyl substituent. It is therefore expected that the oxidation behavior of those terthiophenes with

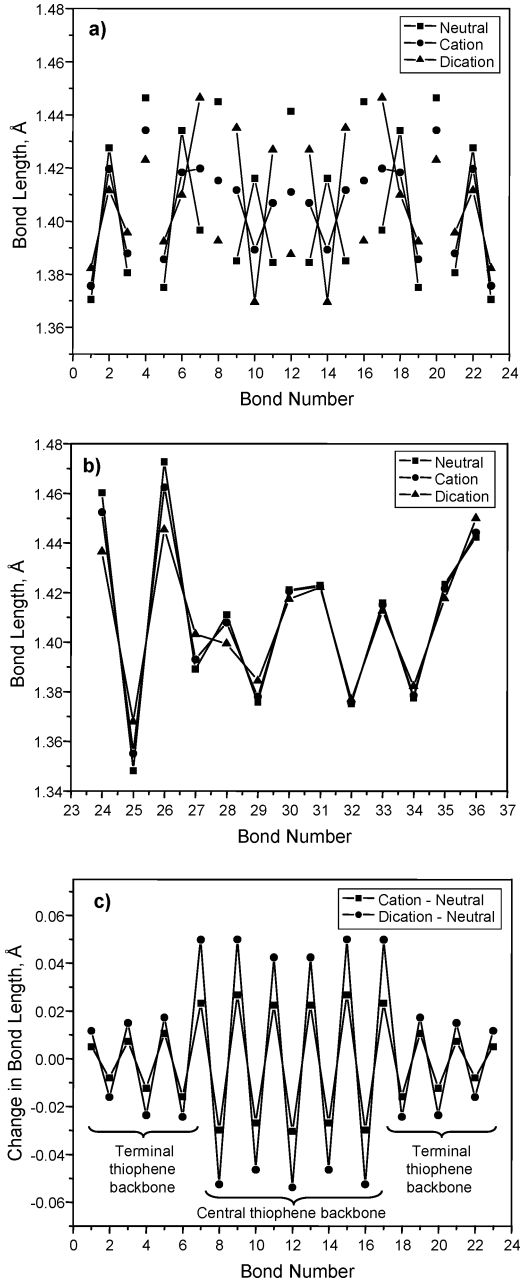

Figure 3. Calculated (B3LYP/3-21G(d)) CC bond length alternation diagram for the sexithiophene backbone (a) and the naphthylethenyl group (b) of (naph-e-3T)$_2$ and its charged species, using the bond numbering system depicted in Figure 3. Each set of three connected symbols represents a thiophene ring, and unconnected symbols represent the inter-ring bonds. The changes in bond length along the sexithiophene backbone (c) between the charged and neutral species are also shown.

large aryl groups will differ from that of the styryl terthiophenes. This is particularly evident from an examination of the spin densities at the thiophene terminal C$_\alpha$ atoms. The cation naph-e-3T$^{\bullet+}$, for instance, has a total spin density of 0.26 at its thiophene C$_\alpha$ termini, indicating both a high reactivity and a tendency for σ-dimerization to occur at these sites. However, this value decreases to 0.17 in anth-e-3T$^{\bullet+}$, suggesting that σ-dimerization is less likely to occur through the thiophene termini.

The spin densities of (anth-e-3T)$_2^{\bullet+}$ (Table S2) reveal the same trends that are observed for the anth-e-3T; i.e., the localization of the spin density shifts from the thiophene backbone to the arylethenyl substituent. The spin density on the substituent almost doubles from (naph-e-3T)$_2^{\bullet+}$ to (anth-e-

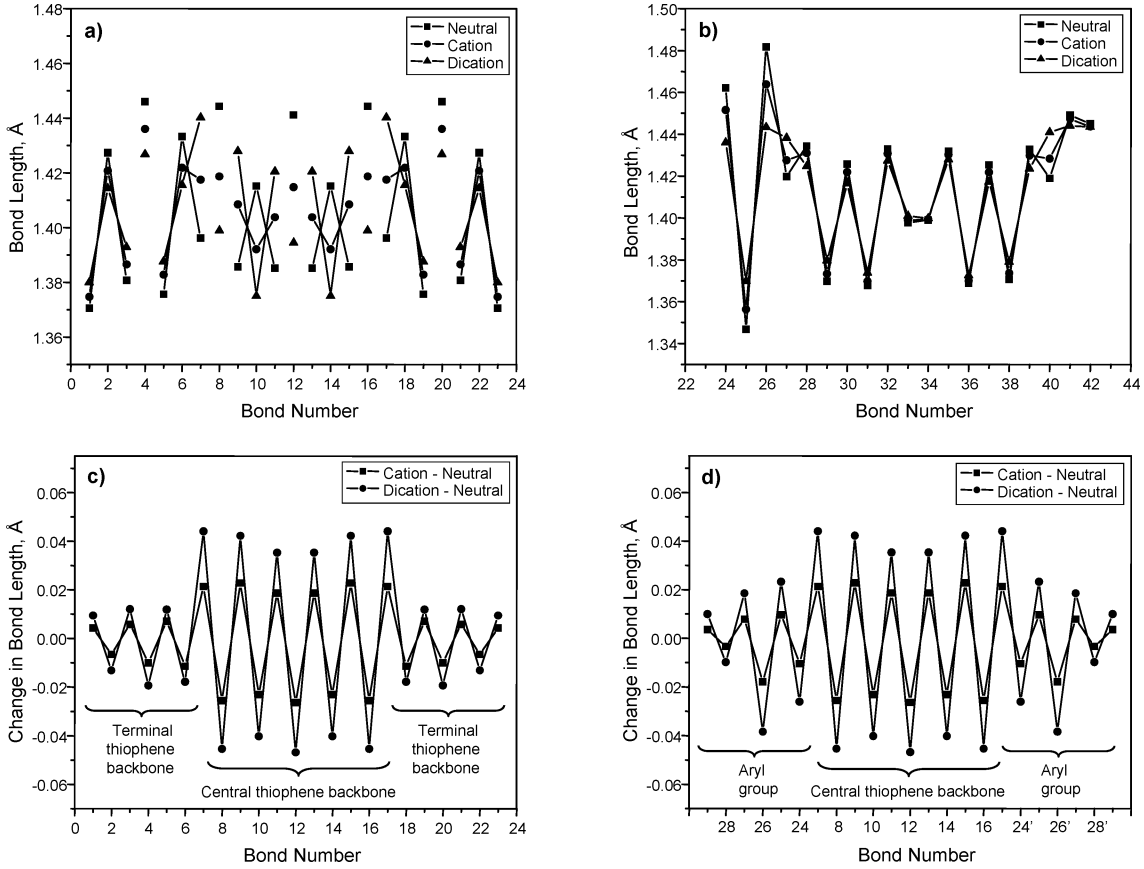

Figure 4. Calculated (B3LYP/3-21G(d)) CC bond length alternation diagram for the sexithiophene backbone (a) and the anthracenylethenyl group (b) of $(anth\text{-}e\text{-}3T)_2$ and its charged species, using the bond numbering system depicted in Figure 3. The changes in bond length along the sexithiophene backbone (c) and along the "aryl-bithiophene-aryl" conjugation path (d) between the charged and neutral species are also shown.

$3T)_2^{\bullet+}$, whereas the spin density on the terminal thiophene rings decreases progressively across the series.

D. Electronic Absorption Spectroscopy of the Neutral Species. The electronic absorption spectrum of naph-e-3T (Figure 5) is similar to that of phenyl-e-3T,[55,56] except that the bands are red-shifted and the low-energy shoulder is less pronounced. The absorption maximum of naph-e-3T is located at 3.72 eV with a shoulder at approximately 3.40 eV. The red shift of both bands is likely to be a result of the increased effective conjugation length imparted by the larger naphthyl group and this is also predicted by the TD-DFT calculations (all TD-DFT and experimental data are presented in Table 2). Two intense transitions are calculated for neutral naph-e-3T at 3.13 and 3.54 eV (f = 0.43 and 0.73, respectively), which correspond to the experimentally observed shoulder and absorption maximum respectively. The estimated experimental oscillator strengths for these transitions are somewhat stronger than those calculated, but the relative intensities are qualitatively predicted (Table 2). As is the case with phenyl-e-3T, the lowest energy transition of naph-e-3T is due to the HOMO → LUMO excitation and the more intense band predicted at 3.54 eV is due to the HOMO−1 → LUMO/HOMO → LUMO+1 configuration. All four of these molecular orbitals (shown in Figure S3) are fairly delocalized, although it seems that the terthiophene backbone has a higher orbital density than the arylethenyl substituent for the HOMO and LUMO and the reverse is true for the HOMO−1 and LUMO+1 (this was also observed for phenyl-e-3T).

The electronic absorption spectrum of naph-e-1T (Figure 5) has a number of differences compared to naph-e-3T. The absorption maximum at 3.84 eV does not have a low-energy shoulder but a high-energy shoulder (on the solvent absorption) is visible instead at 4.63 eV. The TD-DFT calculation on this molecule (Table 2) is consistent with these experimental results. A single transition of high oscillator strength (f = 0.57) is predicted at 3.66 eV, which correlates well with the strong measured absorption band at 3.84 eV. This band can therefore be assigned to the HOMO → LUMO transition. The only other excited state predicted to have a reasonable oscillator strength is that at 4.64 eV (f = 0.16), and it is possible that this excited state is responsible for the measured shoulder at 4.63 eV. The CI coefficients of this latter excited-state indicate an equivalent contribution from three configurations: HOMO−3 → LUMO, HOMO−1 → LUMO, and HOMO → LUMO+1. All of these molecular orbitals are calculated to be delocalized over the whole molecule (Figure S3) with the exception of the LUMO, which is primarily based on the naphthyl group. As separate entities, thiophene and naphthalene absorb at 4.34 and 5.36 eV, respectively.[64] The significant red-shifting that occurs when the two are joined via an ethenyl bridge (to 323 nm) suggests a high level of interaction between the two moieties, which is also reflected in the delocalized molecular orbitals.

The electronic absorption spectra of the anthracenyl-substituted molecules anth-e-1T and anth-e-3T, displayed in Figure 5, are quite different from that of their naphthenyl counterparts. The spectrum of anth-e-1T reveals an absorption maximum at 3.19 eV with numerous shoulders on each side, the most prominent located on the high-energy side at 3.51 and 3.33 eV. Other shoulders are visible at 4.32 and 4.15 eV on top of the solvent absorbance. The absorption maximum, attributed to the HOMO → LUMO transition, is significantly red-shifted compared to that of naph-e-1T (which was located

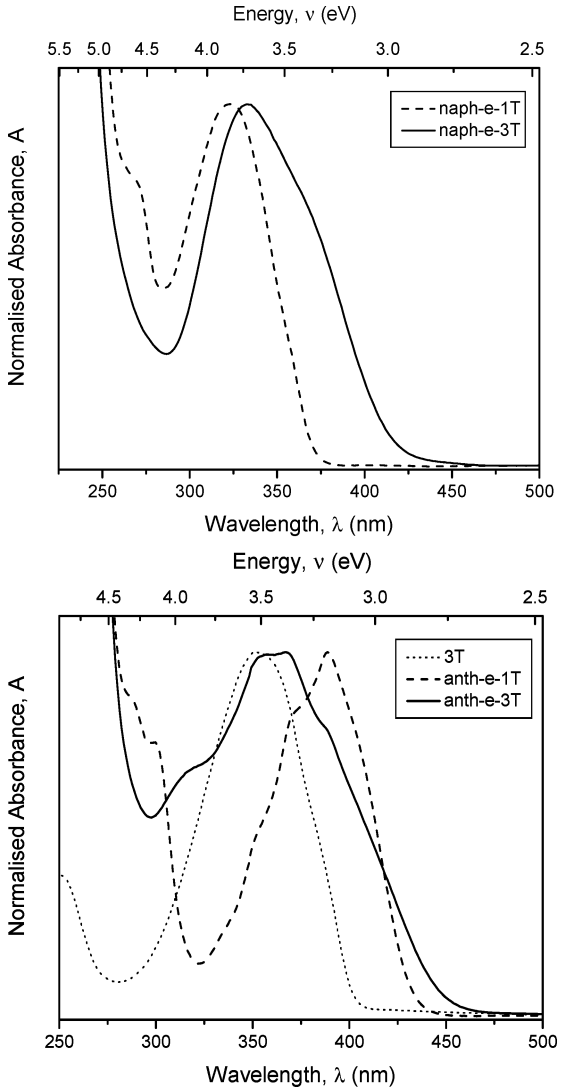

Figure 5. Comparison of the measured electronic absorption spectra of the neutral thiophene naph-e-1T and its terthiophene analogue naph-e-3T (top); a comparison of the measured electronic absorption spectra of the neutral thiophene anth-e-1T, its terthiophene analogue anth-e-3T, and unsubstituted terthiophene (3T, bottom). All spectra are measured in dichloromethane with the absorbance normalized to 1 for each absorption maximum.

at 3.84 eV). The magnitude of this red shift is well predicted by the TD-DFT calculation (Table 2): the measured red shift of the maximum is 0.65 eV and is predicted to be 0.69 eV. The lack of other calculated transitions in this region, however, indicates that the high-energy shoulders on the absorption maximum of anth-e-1T are vibronic in origin. The separation of 1200−1350 cm^{-1} between peaks is consistent with this. In contrast, no vibronic structure is evident in the absorption spectrum of naph-e-1T. The other higher energy peaks in the anth-e-1T spectrum at 4.15 and 4.32 eV can possibly be assigned to a predicted transition at 3.94 eV, which is due to a mixed transition of HOMO−1 → LUMO and HOMO → LUMO+1 excitations. The four molecular orbitals involved in the two electronic transitions of anth-e-1T, displayed in Figure 6, are much more spatially segregated than was observed in the case of naph-e-1T, with the HOMO and LUMO of anth-e-1T primarily localized on the anthracene and the HOMO−1 and LUMO+1 on the thiophene.

The red shift observed in the electronic absorption spectrum of anth-e-3T (shown in Figure 5) relative to naph-e-3T is smaller than that observed between anth-e-1T and naph-e-1T. The main absorption band of anth-e-3T is composed of several transitions, with absorption maxima at 3.46 and 3.38 eV (of almost equivalent absorbance) and shoulders at 3.84 and 3.19 eV. The absorption maximum of naph-e-3T is located at 3.72 eV; thus a red shift of only 0.34 eV is present, compared to the 0.65 eV red shift measured between anth-e-1T and naph-e-1T. It is also interesting to note that anth-e-3T's 3.19 eV shoulder is at the same wavelength as the absorption maximum for anth-e-1T. In addition, the absorption maximum of anth-e-3T at 3.46 eV is at approximately the same wavelength as that of unsubstituted terthiophene (3.53 eV). Indeed, if the absorption spectra of unsubstituted terthiophene and anth-e-1T are averaged together, the resultant spectrum is quite similar to that of anth-e-3T. The only band not taken into account by this addition is the 3.84 eV shoulder. This therefore suggests that the anthracene and terthiophene moieties are potentially electronically *decoupled* within the molecule. Indeed, anthracene itself absorbs at 3.31 and 4.84 eV;[64] thus this chromophore may be a strong contributor to the transitions responsible for the bands at 3.38 and 4.79 eV. The TD-DFT calculation shows three transitions of reasonable oscillator strength (Table 2). These are calculated at 2.79, 3.21, and 3.52 eV (f = 0.30, 0.23, and 0.39, respectively). The lowest energy transition is solely HOMO → LUMO in character and the 3.21 eV transition is of mixed configuration: HOMO−1 → LUMO/HOMO → LUMO+1. The third transition at 3.52 eV, however, is due to a HOMO−1 → LUMO+1 excitation, which has not been predicted for any of the previous oligothiophenes. The calculated molecular orbitals, shown in Figure 6, are quite similar to those of anth-e-1T and reveal the same spatial partitioning, with the HOMO and LUMO localized mainly on the anthracene group and the HOMO−1 and LUMO+1 localized mostly on the terthiophene backbone. The two most intense calculated transitions (the HOMO → LUMO and HOMO−1 → LUMO+1 transitions) therefore involve excitations localized solely on one region within the molecule, either the terthiophene or the anthracene, supporting the potential electronic decoupling observed experimentally. The similarities between the corresponding molecular orbitals of anth-e-1T and anth-e-3T indicate that the extension of the thiophene backbone has only a small effect on the electronic properties of the anthracene group. In contrast, the MOs of naph-e-1T and naph-e-3T are quite different from one another, suggesting a greater interaction between the two sections of the molecule.

E. Electronic Absorption Spectroscopy of the Oxidized Species. The oxidation of naph-e-3T, the results of which are displayed in Figure 7, produces the naphthylethenylsexithiophene $(naph\text{-}e\text{-}3T)_2$. Two bands are measured at 2.82 and 3.69 eV upon reduction, wavelengths similar to those of $(phenyl\text{-}e\text{-}3T)_2$. This therefore shows that the replacement of the phenyl ring with a naphthalene has little effect on the spectral signature of the "styryl" sexithiophene. Generation of the sexithiophene dication is highly facile for this system: when 10^{-5} mol L^{-1} naph-e-3T is oxidized, $(naph\text{-}e\text{-}3T)_2^{2+}$ is formed immediately with an intense band at 1.26 eV and a shoulder at ~1.36 eV. The breadth and intensity of the dication absorption band do not allow for easy identification of the sexithiophene radical cation, $(naph\text{-}e\text{-}3T)_2^{\bullet+}$, bands. However, decay over time of the dication band eventually provided this information (0.95 and 1.65 eV, Figure 7a). Increasing the naph-e-3T concentration to 10^{-4} mol L^{-1} (Figure 7b) allows the π-dimer form of the sexithiophene radical cation, $((naph\text{-}e\text{-}3T)_2^{\bullet+})_2$, to be observed. Its absorption bands are measured at 1.08 and 1.82 eV before the dication band begins to appear. This does not occur for phenyl-e-3T,

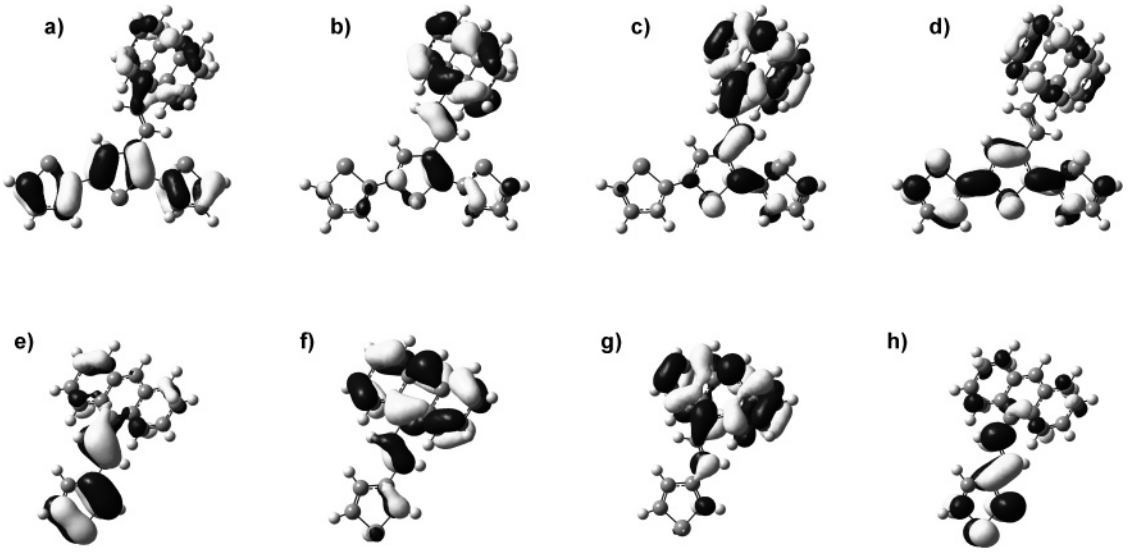

Figure 6. Comparison of the calculated molecular orbitals (B3LYP/6-31G(d)) of neutral anth-e-3T and anth-e-1T involved in their pertinent electronic transitions: HOMO−1 (a), HOMO (b), LUMO (c), and LUMO+1 (d) of anth-e-3T; HOMO−1 (e), HOMO (f), LUMO (g), and LUMO+1 (h) of anth-e-1T.

TABLE 2: Vertical Transition Energies, Oscillator Strengths (*f*), and Configurations of the Excited States Calculated for the Neutral Compounds Using TD-DFT (B3LYP/6-31G(d)) and Compared to the Measured Electronic Absorption Data

	experimental transition energy (extinction coefficient/10^3 L mol^{-1}cm^{-1})					
molecule	nm	eV	calcd transition energy (eV)	oscillator strength, *f* calcd (expt)	transition	CI coeff
naph-e-3T	365 (154)	3.40	3.13	0.43 (1.2)	HOMO → LUMO	0.64
	333 (210)	3.72	3.54	0.73 (1.6)	HOMO → LUMO+1	−0.31
					HOMO−1 → LUMO	0.57
naph-e-1T	323 (156)	3.84	3.66	0.57 (1.8)	HOMO → LUMO	0.64
	267 (124)	4.63	4.64	0.16 (1.3)	HOMO−3 → LUMO	0.40
					HOMO → LUMO+1	0.36
					HOMO−1 → LUMO	−0.32
anth-e-1T	389 (72)	3.19	2.97	0.25 (0.68)	HOMO → LUMO	0.64
	372 (60)	3.33				
	353 (37)	3.51				
	299 (55)	4.15	3.94	0.14 (0.27)	HOMO → LUMO+1	0.48
					HOMO−1 → LUMO	−0.44
	287 (64)	4.32				
anth-e-3T	389 (128)	3.19	2.79	0.30 (0.64)	HOMO → LUMO	0.65
	367 (162)	3.38	3.21	0.23 (0.81)	HOMO → LUMO+1	−0.31
					HOMO−1 → LUMO	0.57
	358 (162)	3.46	3.52	0.39 (0.81)	HOMO−1 → LUMO+1	0.66
	323 (112)	3.84		(0.56)		

for which no sexithiophene dication formation is evident when the high substrate concentration (10^{-4} mol L^{-1}) is oxidized.

When anth-e-3T is oxidized, however, a completely different behavior is observed that does not occur for any of the other arylethenyl terthiophenes and sexithiophenes, as illustrated in Figure 8. A very intense absorption band at 1.82 eV appears upon oxidation. This band is also accompanied by another at ∼1.24 eV, the relative intensity of which depends on the substrate and oxidant concentration. The two-band feature indicative of the "styryl" sexithiophene does not occur when this oxidized state is reduced with hydrazine, implying that the oxidized species formed is not of sexithiophene origin. Neither is the anthracenylethenyl terthiophene regenerated. It has been previously established that the anthracene radical cation absorbs strongly at 1.72 eV.[65,66] It is therefore possible that the band at 1.82 eV is caused by a derivative of the anthracene radical cation. This possibility is supported by the calculated spin density results, which showed that the majority of the anth-e-3T cation's spin is localized on the anthracene moiety. The origin of the ∼1.24 eV band is unknown, but it is possible that it is caused by transitions associated with the thiophene backbone. In addition to this, a number of experimental studies have demonstrated that anthracene can form a σ-dimer.[67−70] The optical spectrum of 9,9′-bianthracene has been measured and bands are observed at 1.81 and 1.67 eV in CH_2Cl_2[69] and 1.74 eV in MeCN.[71] It is thus reasonable to suggest that the observed optical spectrum for oxidized anth-e-3T contains contributions from products associated with the anthracene moiety.

F. Cyclic Voltammetry. Compound naph-e-3T reveals a cyclic voltammogram (shown in Figure 9a) that possesses a number of similarities to that of phenyl-e-3T. From both the increasing current with consecutive cycles and the appearance of anodic peaks of lower potential than the initial one,[55,72,73] it can be concluded that a film of (naph-e-3T)$_2$ sexithiophene charged species is growing on the working electrode surface. The initial terthiophene oxidation is measured at $E_{pa} = 1.14$ V, a slightly lower potential than that of phenyl-e-3T ($E_{pa} = 1.17$ V). Similarly, the oxidation potentials for the generation of the sexithiophene radical cation and dication are also slightly lower for (naph-e-3T)$_2$ ($E_{pa} = 0.82$ and 1.03 V) than is observed for

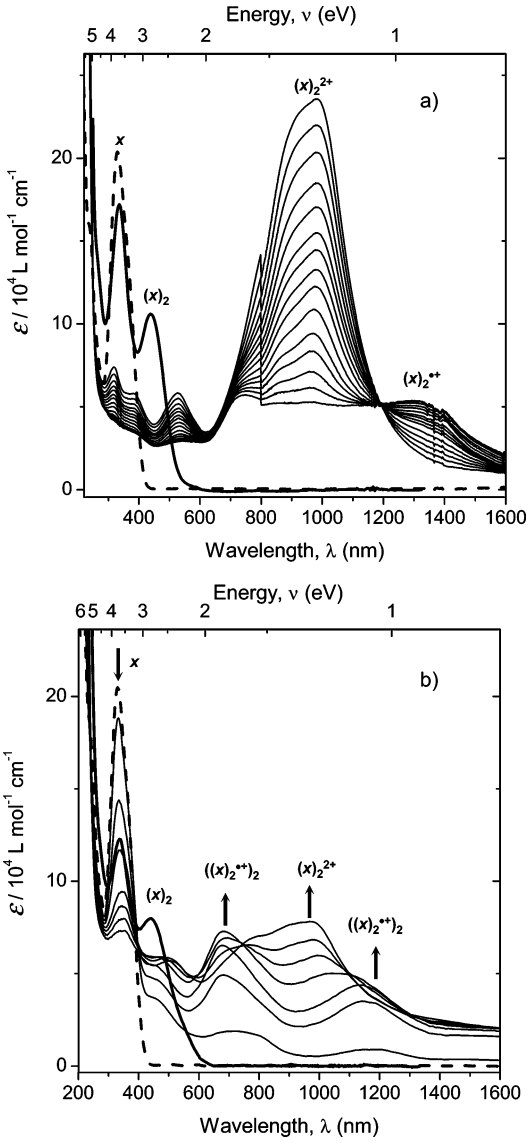

Figure 7. Evolution of the electronic absorption spectra during the chemical oxidations of 10^{-5} mol L^{-1} (a) and 10^{-4} mol L^{-1} (b) naph-e-3T using an 8×10^{-4} mol L^{-1} solution of $Cu(ClO_4)_2$ in acetonitrile. The spectra shown in bold type are those of the neutral terthiophene species (---) and the product of the reduction of the end oxidation product with aqueous hydrazine (—). Note that (a) shows the decay over time of the dication band to reveal the radical cation absorption bands. The different species are labeled, where x = naph-e-3T.

(phenyl-e-3T)$_2$ (E_{pa} = 0.84 and 1.06 V). The two cathodic peaks are clearly defined at E_{pc} = 0.72 and 0.98 V.

The cyclic voltammogram of the thiophene naph-e-1T (Figure 9b) is quite different from the CV of its terthiophene analogue, naph-e-3T. Two anodic peaks are measured for naph-e-1T at E_{pa} = 1.35 and 1.49 V. These oxidation potentials are appreciably higher than that of the terthiophene oxidation (E_{pa} = 1.14 V), an observation consistent with the lower stability of the charged species. In addition, the oxidation of the thiophene naph-e-1T is completely irreversible, with no cathodic peaks in evidence and subsequent scans show that the original anodic peaks have been lost. It therefore seems likely that the naph-e-1T oxidized species are unstable and rapidly degrade to form unknown products.

In contrast, the cyclic voltammograms of anth-e-1T and anth-e-3T (Figure 9c,d) reveal similar patterns, suggesting that it is the anthracenyl moiety that dominates the redox behavior rather than the length of the thiophene chain. This is consistent with

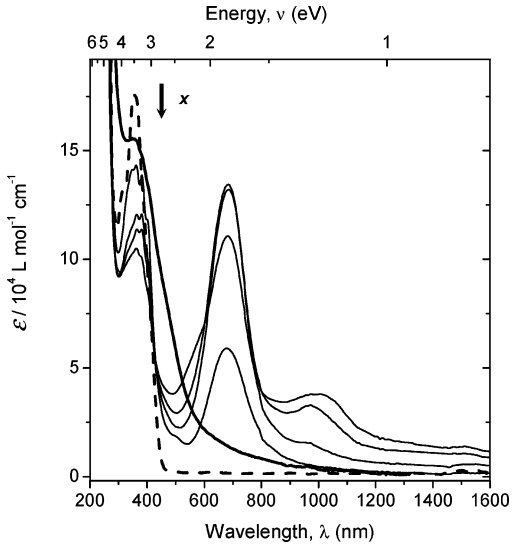

Figure 8. Evolution of the electronic absorption spectra during the chemical oxidation of 10^{-5} mol L^{-1} anth-e-3T using an 8×10^{-4} mol L^{-1} solution of $Cu(ClO_4)_2$ in acetonitrile. The spectra shown in bold type are those of the neutral terthiophene species (---) and the product of the reduction of the end oxidation product with aqueous hydrazine (—).

earlier studies that show that anthracene may form σ-dimers when oxidized.[68] Both CVs show two anodic peaks between 1.00 and 1.45 V, with those of the terthiophene anth-e-3T at a lower potential (E_{pa} = 1.09 and 1.26 V) than anth-e-1T (E_{pa} = 1.16 and 1.38 V), a result of the increased conjugation length allowing a greater stabilization of the charged species that form. Note that the two anodic peaks of anth-e-1T occur at lower potentials than the corresponding peaks in the naphthyl-substituted naph-e-1T's CV, which is also a result of the extension of the ring system. Both anth-e-1T and anth-e-3T have another anodic peak at higher potential (E_{pa} = 1.50 and 1.70 V, respectively), but the origin of this third peak is unclear. The oxidation of these two compounds is quasi-reversible to irreversible, with only very indistinct cathodic processes observed at E_{pc} = 1.25 and 1.41 V for anth-e-1T and E_{pc} = 0.69 and 1.40 V for anth-e-3T.

G. Raman Spectra of Neutral Terthiophenes. The measured Raman spectrum of naph-e-3T, shown in Figure 10a, is dominated by vibrations localized on the terthiophene unit rather than the naphthylethenyl group. These include the very intense $\nu_s(C{=}C)_{3T}$ vibrational mode at 1459 cm^{-1} (line B), which is both predicted (at 1445 cm^{-1}, Figure 10b) and observed experimentally as the strongest band in the Raman spectrum, and a $\nu_{as}(C{=}C)_{3T}$ mode measured at 1521 cm^{-1} and calculated at 1523 cm^{-1}, respectively (line A). The $\nu_s(CC)_{naphthalene}$ mode calculated at 1562 cm^{-1} and observed at 1573 cm^{-1} and the $\nu(C{=}C)_{ethenyl}$ mode predicted at 1619 cm^{-1} and measured at 1621 cm^{-1} have moderate intensity.

The nature of the modes in the calculated Raman spectrum of anth-e-3T (Figure 10d) are in general very similar to those of naph-e-3T. The $\nu_s(C{=}C)_{3T}$ vibrational mode is once again predicted to be the most intense band. Its localization entirely on the terthiophene backbone ensures that the replacement of the naphthalene substituent by an anthracene does little to affect the frequency of the mode: it is predicted at 1447 cm^{-1} and measured at 1462 cm^{-1} for anth-e-3T (Figure 10c), deviations of only 2 and 3 cm^{-1}, respectively, from that of naph-e-3T. However, this is not the case for line A; although it is predicted at 1523 cm^{-1} for both molecules, it is upshifted by 10 cm^{-1} to 1531 cm^{-1} in the measured Raman spectrum of anth-e-3T. The

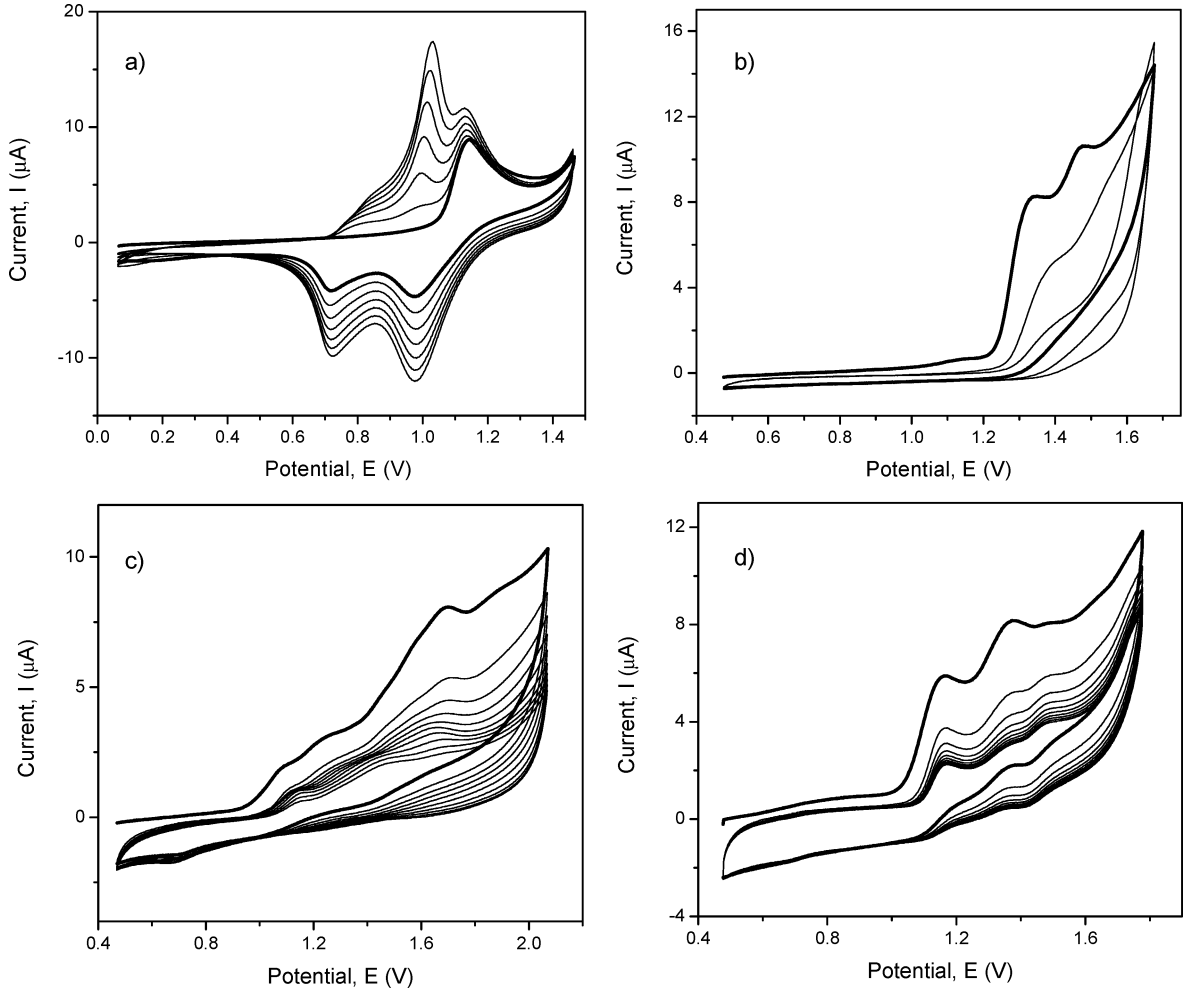

Figure 9. Cyclic voltammograms of 5×10^{-4} mol L^{-1} naph-e-3T (a), 1×10^{-3} M naph-e-1T (b), 5×10^{-4} mol L^{-1} anth-e-3T (c), and 5×10^{-4} mol L^{-1} anth-e-1T (d) in 0.1 mol L^{-1} TBAP/acetonitrile with scan rates of 0.8, 0.2, 0.5, and 2.0 V s^{-1}, respectively. Potentials vs Ag/AgCl and calibrated against $Me_{10}Fc^{+/0}$. The CVs in bold type represent the first scan for each compound.

downshift of the $\nu_s(C{=}C)_{aryl}$ mode from naph-e-3T to anth-e-3T can be observed in both the experimental (from 1573 to 1558 cm^{-1}) and theoretical Raman spectra (1562 to 1544 cm^{-1}). It is likely that this is a consequence of the increased conjugation imparted by the larger anthracene ring system. This continues the trend seen for this mode from phenyl-e-3T to naph-e-3T. The $\nu_s(C{=}C)_{phenyl}$ mode of phenyl-e-3T is predicted at 1593 cm^{-1} and measured at 1598 cm^{-1}, producing predicted/measured downshifts of 31/25 cm^{-1} from phenyl-e-3T to naph-e-3T, and then 18/15 cm^{-1} from naph-e-3T to anth-e-3T.

H. Raman Spectra of Neutral Sexithiophenes. The theoretical vibrational spectra of $(naph\text{-}e\text{-}3T)_2$ were calculated using both 6-31G(d) and 3-21G(d) basis sets, and the larger sexithiophene $(anth\text{-}e\text{-}3T)_2$ required the smaller 3-21G(d) basis set due to its size. The calculated and measured Raman spectra of $(naph\text{-}e\text{-}3T)_2$ are presented in Figure 11; those of $(anth\text{-}e\text{-}3T)_2$ are shown in Figure S4.

As was observed with styryl sexithiophenes such as $(phenyl\text{-}e\text{-}3T)_2$,[54] the $\nu_s(C{=}C)_{6T}$ vibrational modes are predicted to be very strong in the Raman spectrum of $(naph\text{-}e\text{-}3T)_2$ (Figure 11). Two very intense modes are calculated using the 6-31G(d) basis set at 1432 and 1441 cm^{-1}. The latter band is a $\nu_s(C{=}C)_{6T}$ mode coupled to a small asymmetric motion of the naphthalene group, and the former mode is localized solely on the sexithiophene backbone. The corresponding modes in the $(phenyl\text{-}e\text{-}3T)_2$ calculated Raman spectrum are predicted at 1431 and 1435 cm^{-1};[55] i.e., the $\nu_s(C{=}C)_{6T}$ mode coupled to the aryl group motion upshifts by 6 cm^{-1} when the phenyl ring is replaced by a naphthalene. The measured Raman spectrum of the $(naph\text{-}e\text{-}3T)_2$ neutral film shows one very broad intense band centered at 1469 cm^{-1}; its breadth suggests that it encompasses a number of modes, but overall it can be assigned to a primarily $\nu_s(C{=}C)_{6T}$ vibrational mode. The Raman spectrum of the $(phenyl\text{-}e\text{-}3T)_2$ film[54] also has this broad intense band, but it is centered at lower energy (1461 cm^{-1}): this upshift from $(phenyl\text{-}e\text{-}3T)_2$ to $(naph\text{-}e\text{-}3T)_2$ is consistent with the predicted contribution from the coupled aryl asymmetrical stretching vibration. The second strongest mode in the theoretical spectrum (although only 14% of the calculated intensity of the $\nu_s(C{=}C)_{6T}$ modes) is line D, the $\delta(CH)_{6T}$ mode localized only on the central two thiophene rings; it is predicted at 1044 cm^{-1} and measured at 1051 cm^{-1}. This has downshifted slightly from that measured for the styryl sexithiophenes, 1058 cm^{-1} in the case of $(phenyl\text{-}e\text{-}3T)_2$, although they are predicted at virtually the same frequency. The other predicted bands in the $(naph\text{-}e\text{-}3T)_2$ Raman spectrum are comparatively very weak, less than 9% of the intensity of the $\nu_s(C{=}C)_{6T}$ modes. These include the $\nu_s(CC)_{naphthalene}$ mode calculated at 1562 cm^{-1} and observed at 1573 cm^{-1}. As was observed for the corresponding terthiophenes, this $\nu_s(CC)_{naphthalene}$ mode is downshifted both theoretically and experimentally from the corresponding $\nu_s(CC)_{phenyl}$ mode of $(phenyl\text{-}e\text{-}3T)_2$, which was predicted at 1593 cm^{-1} and measured at 1598 cm^{-1}. The $\nu_s(C{=}C)_{aryl}$ mode does not shift from naph-e-3T to $(naph\text{-}e\text{-}3T)_2$ (or from phenyl-e-3T to $(phenyl\text{-}e\text{-}3T)_2$), however; thus

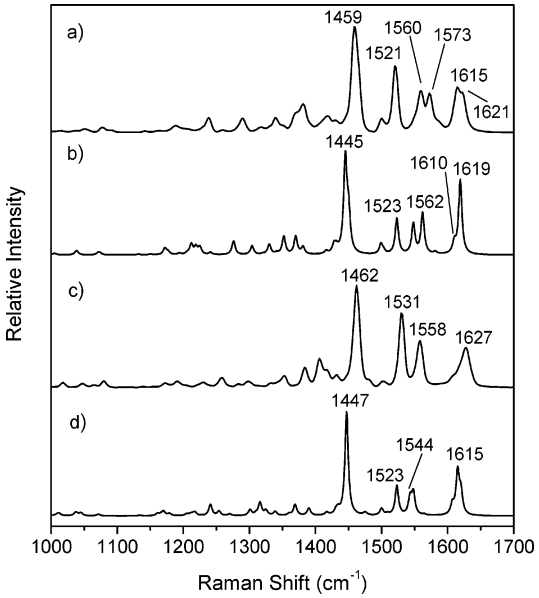

Figure 10. Comparison of the experimental FT-Raman (a) with the theoretical B3LYP/6-31G(d) Raman spectrum (b) of neutral naph-e-3T and comparison of the experimental FT-Raman (c) with the theoretical B3LYP/6-31G(d) Raman spectrum (d) of neutral anth-e-3T. The FT-Raman spectra were measured of a pure solid samples using $\lambda_{exc} = 1064$ nm. Numbers denote the frequency of the bands in wavenumbers (cm^{-1}).

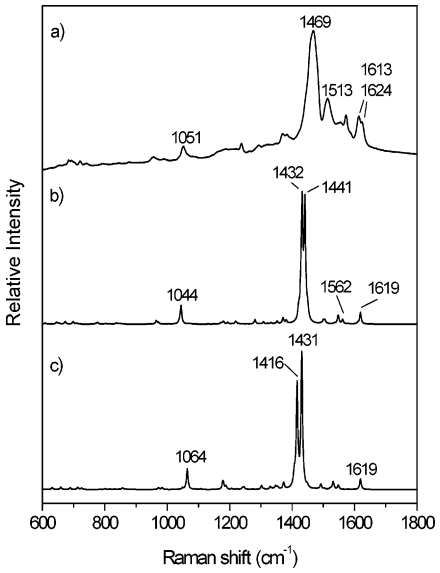

Figure 11. Comparison of the experimental resonance Raman ($\lambda_{exc} =$ 413 nm) spectrum of the film generated from the electrochemical oxidation and then reduction of a naph-e-3T solution onto ITO (a) with the theoretical B3LYP/6-31G(d) (b) and 3-21G(d) (c) Raman spectra of $(naph\text{-}e\text{-}3T)_2$. Numbers denote the frequency of the bands in wavenumbers (cm^{-1}).

the magnitude of the downshift remains the same. In turn, this indicates a lack of vibrational coupling between the two aryl units of the sexithiophene.

The two calculated Raman spectra of $(naph\text{-}e\text{-}3T)_2$ using the basis sets 3-21G(d) and 6-31G(d) are very similar (Figure 11), both having two strong bands between 1415 and 1445 cm^{-1}. When the $\nu(C{=}C)_{ethenyl}$ mode is set at 1619 cm^{-1} as the reference point for the 3-21G(d) scale factor, the sexithiophene-based stretching modes are significantly downshifted relative to 6-31G(d). For instance, the two intense $\nu_s(C{=}C)_{6T}$ modes shift from 1432 and 1441 cm^{-1} (6-31G(d)) to 1416 and 1431 cm^{-1} (3-21G(d)), respectively. Their intensities also alter between the two basis sets: in the 6-31G(d) Raman spectrum the two bands are of approximately the same intensity whereas 3-21G(d) predicts the $\nu_s(C{=}C)_{6T}$ mode localized primarily on the central two thiophene rings at 1416 cm^{-1} to be lower in intensity. The higher energy $\nu_s(C{=}C)_{6T}$ mode is predicted by both basis sets to be delocalized over the full sexithiophene backbone.

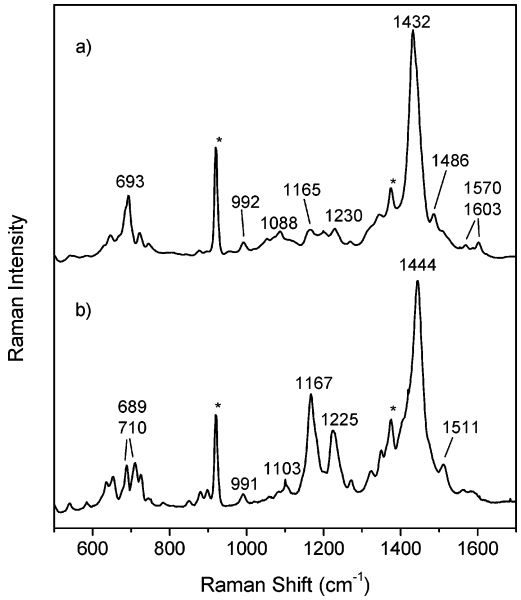

Figure 12. Experimental solution Raman spectra of the first (a) and second (b) oxidation stages of naph-e-3T with $Cu(ClO_4)_2$/AcN using an excitation wavelength of $\lambda_{exc} = 752$ nm, with an initial naph-e-3T concentration of 2×10^{-5} mol L^{-1}. Asterisks denote solvent bands.

The 3-21G(d) calculated Raman spectrum of $(anth\text{-}e\text{-}3T)_2$ (Figure S4) shows few differences from that of $(naph\text{-}e\text{-}3T)_2$. The two intense sexithiophene-localized bands dominate the spectra, unshifted from $(naph\text{-}e\text{-}3T)_2$ at 1415 and 1430 cm^{-1} for both molecules. The resonance Raman spectrum of the anth-e-3T oxidized/reduced film is indicative of a styrylsexithiophene with regard to the single intense band at 1469 cm^{-1} and a weaker overlapping band at 1516 cm^{-1}, but the absence of the higher energy arylethenyl stretching modes suggests the possibility of other processes occurring as well.

I. Raman Spectroscopy of Oxidized Species. Oxidation of naph-e-3T in solution produces clear evidence of sexithiophene radical cation and dications in the solution state resonance Raman spectra, as shown in Figure 12. Indeed, these spectra are very similar to those of oxidized $(phenyl\text{-}e\text{-}3T)_2$,[54] indicating that the replacement of the phenyl ring with a naphthalene has little effect on the vibrational properties of the charged species. However, the intense thiophene inter-ring CC stretching mode of the $(naph\text{-}e\text{-}3T)_2$ radical cation does downshift slightly to 1432 cm^{-1} compared to that of $(phenyl\text{-}e\text{-}3T)_2^{\bullet+}$ (1436 cm^{-1}). This does not occur for the dication and the bands of both molecules are at the same frequency (1445 cm^{-1}). The $(naph\text{-}e\text{-}3T)_2^{\bullet+}$ band at 693 cm^{-1} has also downshifted from its counterpart at 702 cm^{-1} in the $(phenyl\text{-}e\text{-}3T)_2^{\bullet+}$ Raman spectrum. This also occurs for alkoxy-substituted styryl sexithiophenes[54] and suggests that the vibrational mode responsible has some influence from the "styryl" substituents. The eigenvectors of the vibrational modes present in this region of the calculated spectra of $(phenyl\text{-}e\text{-}3T)_2^{\bullet+}$ and $(naph\text{-}e\text{-}3T)_2^{\bullet+}$ reveal that although C−S stretching is the dominant motion, some aryl ring breathing is also present, thus accounting for this mode's sensitivity to substitution.

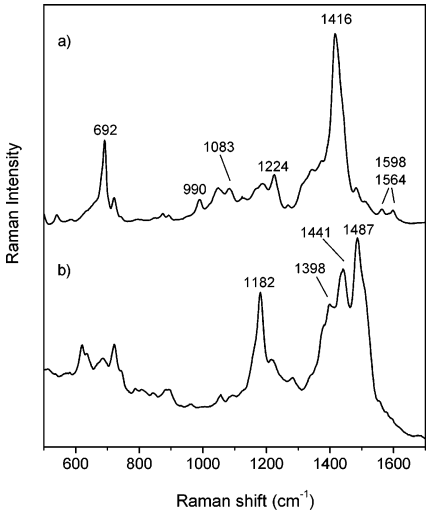

Figure 13. Experimental solid-state Raman spectra of oxidized films created by the electrochemical oxidation of naph-e-3T (a) and anth-e-3T (b) using an excitation wavelength of $\lambda_{exc} = 752$ nm.

The $\nu(C{=}C)_{ethenyl}/\nu_s(CC)_{aryl}$ mode of (naph-e-3T)$_2$ undergoes a downshift upon formation of the radical cation, as was observed for the dimethyl end-capped phenyl-e-3T[74] and the styryl sexithiophenes.[54] However, the frequency shift measured for (naph-e-3T)$_2$ is appreciably larger than any of the previous compounds discussed. The neutral band of (naph-e-3T)$_2$ at 1624 cm^{-1} shifts to 1603 cm^{-1} for (naph-e-3T)$_2^{\bullet+}$; the large 21 cm^{-1} downshift reflects the fact that the naphthalene unit causes the charged defect to partially extend into the substituents rather than completely along the sexithiophene backbone. This is consistent with the calculated reduction in spin and bond length changes associated with the thiophene rings and the increase in these parameters associated with the naphthylethenyl substituents. Indeed, the downshift observed for (naph-e-3T)$_2$ is even larger than that of the dimethyl end-capped phenyl-e-3T,[74] where the structural defect of the radical cation is confined to a very small area and must by necessity extend into the styryl group to fulfill its space requirements.

Despite this effect of the naphthalene units, the resonance Raman spectra of (naph-e-3T)$_2^{\bullet+}$ and (naph-e-3T)$_2^{2+}$ are still very similar to those of (phenyl-e-3T)$_2$ and are thus dominated by the vibrational properties of the sexithiophene backbone. The presence of the naphthalene groups serves only to shift the bands. However, this might not be the case for the anthracenylethenyl species anth-e-3T, where the effect of the larger aryl group on the spin and bond length changes is predicted to be greater than that of the naphthyl substituent. This is evident in the Raman spectra of oxidized anth-e-3T; indeed, the electronic spectra of oxidized anth-e-3T did not indicate the presence of a sexithiophene species. The resonance Raman spectrum of a film of oxidized anth-e-3T (Figure 13b) is consistent with this and the spectral signatures of the "styryl" sexithiophene radical cations and dications are not present. Instead, the most intense band is measured at 1487 cm^{-1}, which has a prominent shoulder at 1505 cm^{-1}. Other strong bands appear at 1182, 1398, and 1441 cm^{-1}. As such, this spectrum is very different from that of the (naph-e-3T)$_2^{\bullet+}$ film (Figure 13a), which has the signature radical cation bands at 690 and 1417 cm^{-1} (downshifted from the corresponding solution state band at 1432 cm^{-1}). It is therefore probable that these new bands of oxidized anth-e-3T are due to vibrational modes associated with the charged anthracenyl moiety.

IV. Conclusions

The results presented in this paper indicate that the two terthiophenes naph-e-3T and anth-e-3T have different structural and electronic properties in both the neutral and charged states. In the case of naph-e-3T, these properties are dominated by the terthiophene backbone, whereas the properties of anth-e-3T are dominated by the anthracene group. This can be seen, for example, in the electronic absorption spectra of the neutral species: the spectrum and electronic transitions of naph-e-3T are similar to phenyl-e-3T (taking into account the red-shifts induced by the increase in conjugation length), but this is not the case for anth-e-3T and anth-e-1T. For the latter two molecules all of the molecular orbitals involved in its low-energy transitions are spatially partitioned, electronically decoupling the anthracene and terthiophene moieties. As a result, the absorption spectrum of anth-e-3T is composed of a simple addition of the absorption bands of the two chromophores. Other experimental evidence for this decoupling phenomenon can be found in the cyclic voltammograms of the two terthiophenes, where a comparison with the cyclic voltammograms of their thiophene analogues has shown that the two anthracenyl compounds have very similar electrochemical properties, suggesting that the extension of the thiophene backbone has little effect.

In both the electronic absorption and resonance Raman spectra of oxidized naph-e-3T, evidence of sexithiophene radical cations and dications is observed. However, these spectral signatures are not present when anth-e-3T is oxidized; instead, it appears as if the anthracene group is the primary site of the structural changes induced by removal of electrons.

DFT calculations support the experimental observations. Both spin density and bond-length-change data indicate that the location of the charged defect on (aryl-e-3T)$_2^{\bullet+/2+}$ shifts from the sexithiophene backbone to the substituent when the aryl group is extended from the naphthalene to the anthracene. This is also apparent for the short-lived terthiophene radical cations, where the predicted higher proportion of spin density on the anthracene of anth-e-3T$^{\bullet+}$ suggests a reduced yield of sexithiophene product upon oxidation.

The effect of aryl substituents on the electronic structure of the terthiophene and sexithiophene species may be summarized as follows: (1) In the neutral species the thiophene backbone and anthracenyl pendent groups are electronically decoupled; (2) In the oxidized species, however, the structure of the charge defect is modulated by the nature of the pendent group. This study thus provides an example of the importance of investigating the nature of the charged species directly rather than surmising the structural behavior on the basis of neutral species calculations. As the conduction mechanism in sexithiophenes is influenced by the nature of the defect and its spatial extent,[75] the defect modulation may influence the ability of anthracenyl-substituted thiophenes to act effectively in molecular electronic devices.

Acknowledgment. The support of the Foundation of Research Science and Technology (NERF), the Royal Society of New Zealand (Marsden Fund), and the MacDiarmid Institute for Advanced Materials and Nanotechnology is gratefully acknowledged.

Supporting Information Available: Experimental crystal structure and calculated structure, bond length alternation diagram, molecular orbital comparison, and resonance Raman

spectra and tables of spin densities. This material is available free of charge via the Internet at http://pubs.acs.org.

References and Notes

(1) Burroughes, J. H.; Bradley, D. D. C.; Brown, A. R.; Marks, R. N.; Mackay, K.; Friend, R. H.; Burns, P. L.; Holmes, A. B. *Nature* **1990**, *347*, 539.

(2) Dai, L.; Winkler, B.; Dong, L.; Tong, L.; Mau, A. W. H. *Adv. Mater.* **2001**, *13*, 915.

(3) Katz, H. E. *J. Mater. Chem.* **1997**, *7*, 369.

(4) Horowitz, G.; Delannoy, P.; Bouchriha, H.; Deloffre, F.; Fave, J. L.; Garnier, F.; Hajlaoui, R.; Heyman, M.; Kouki, F.; et al. *Adv. Mater.* **1994**, *6*, 752.

(5) Garnier, F.; Horowitz, G.; Peng, X.; Fichou, D. *Adv. Mater.* **1990**, *2*, 592.

(6) Horowitz, G.; Garnier, F.; Yassar, A.; Hajlaoui, R.; Kouki, F. *Adv. Mater.* **1996**, *8*, 52.

(7) Fichou, D.; Demanze, P.; Horowitz, G.; Hajlaoui, R.; Constant, M.; Garnier, F. *Synth. Met.* **1997**, *85*, 1309.

(8) Hajlaoui, R.; Fichou, D.; Horowitz, G.; Nessakh, B.; Constant, M.; Garnier, F. *Adv. Mater.* **1997**, *9*, 557.

(9) Hernandez, V.; Casado, J.; Ramirez, F. J.; Zotti, G.; Hotta, S.; Navarrete, J. T. L. *J. Chem. Phys.* **1996**, *104*, 9271.

(10) Hernandez, V.; Casado, J.; Ramirez, F. J.; Alemany, L. J.; Hotta, S.; Lopez Navarrete, J. T. *J. Phys. Chem.* **1996**, *100*, 289.

(11) Hernandez, V.; Casado, J.; Kanemitsu, Y.; Lopez Navarrete, J. T. *J. Chem. Phys.* **1999**, *110*, 6907.

(12) Moreno Castro, C.; Ruiz Delgado, M. C.; Hernandez, V.; Hotta, S.; Casado, J.; Lopez Navarrete, J. T. *J. Chem. Phys.* **2002**, *116*, 10419.

(13) Casado, J.; Hernandez, V.; Kanemitsu, Y.; Navarrete, J. T. L. *J. Raman Spectrosc.* **2000**, *31*, 565.

(14) Casado, J.; Hernandez, V.; Hotta, S.; Lopez Navarrete, J. T. *J. Chem. Phys.* **1998**, *109*, 10419.

(15) Casado, J.; Bengoechea, M.; Lopez Navarrete, J. T.; Otero, T. F. *Synth. Met.* **1998**, *95*, 93.

(16) Casado, J.; Hotta, S.; Hernandez, V.; Navarrete, J. T. L. *Opt. Mater.* **1999**, *12*, 321.

(17) Furukawa, Y. *J. Phys. Chem.* **1996**, *100*, 15644.

(18) Doretto, R. L.; Del Nero, J.; Laks, B. *Synth. Met.* **1999**, *101*, 178.

(19) Stanforth, S. P. *J. Heterocycl. Chem.* **1999**, *36*, 137.

(20) Aleman, C.; Julia, L. *J. Phys. Chem.* **1996**, *100*, 1524.

(21) Casado, J.; Hernandez, V.; Ramirez, F. J.; Navarrete, T. L. *J. Mol. Struct: THEOCHEM* **1999**, *463*, 211.

(22) Ciofalo, M.; La Manna, G. *Chem. Phys. Lett.* **1996**, *263*, 73.

(23) DiCesare, N.; Belletete, M.; Leclerc, M.; Durocher, G. *J. Mol. Struct: THEOCHEM* **1999**, *467*, 259.

(24) Viruela, P. M.; Viruela, R.; Orti, E.; Bredas, J.-L. *J. Am. Chem. Soc.* **1997**, *119*, 1360.

(25) Alberti, A.; Ballarin, B.; Guerra, M.; Macciantelli, D.; Mucci, A.; Parenti, F.; Schenetti, L.; Seeber, R.; Zanardi, C. *ChemPhysChem* **2003**, *4*, 1216.

(26) Bouzzine, S. M.; Bouzakraoui, S.; Bouachrine, M.; Hamidi, M. *J. Mol. Struct: THEOCHEM* **2005**, *726*, 271.

(27) Hernandez, V.; Casado, J.; Favaretto, L.; Distefano, G.; Lopez Navarrete, J. T. *Synth. Met.* **1999**, *101*, 590.

(28) Hernandez, V.; Casado, J.; Lopez Navarrete, J. T. *J. Mol. Struct.* **2000**, *521*, 249.

(29) Ruiz Delgado, M. C.; Casado, J.; Hernandez, V.; Lopez Navarrete, J. T.; Fuhrmann, G.; Baeuerle, P. *J. Phys. Chem. B* **2004**, *108*, 3158.

(30) Howell, S. L.; Gordon, K. C. *J. Phys. Chem. A* **2004**, *108*, 2536.

(31) Stafstroem, S.; Bredas, J. L. *Phys. Rev. B* **1988**, *38*, 4180.

(32) Ehrendorfer, C.; Karpfen, A. *J. Phys. Chem.* **1994**, *98*, 7492.

(33) Ehrendorfer, C.; Karpfen, A. *J. Phys. Chem.* **1995**, *99*, 5341.

(34) Cuff, L.; Kertesz, M. *J. Chem. Phys.* **1997**, *106*, 5541.

(35) Gao, Y.; Liu, C.-G.; Jiang, Y.-S. *J. Phys. Chem. A* **2002**, *106*, 5380.

(36) Casado, J.; Miller, L. L.; Mann, K. R.; Pappenfus, T. M.; Hernandez, V.; Lopez Navarrete, J. T. *J. Phys. Chem. B* **2002**, *106*, 3597.

(37) Cornil, J.; Beljonne, D.; Bredas, J. L. *J. Chem. Phys.* **1995**, *103*, 842.

(38) Becker, R. S.; de Melo, J. S.; Macanita, A. L.; Elisei, F. *J. Phys. Chem.* **1996**, *100*, 18683.

(39) Becker, R. S.; de Melo, S.; Macanita, A. L.; Elisei, F. *Pure Appl. Chem.* **1995**, *67*, 9.

(40) Colditz, R.; Grebner, D.; Helbig, M.; Rentsch, S. *Chem. Phys.* **1995**, *201*, 309.

(41) Graf, D. D.; Duan, R. G.; Campbell, J. P.; Miller, L. L.; Mann, K. R. *J. Am. Chem. Soc.* **1997**, *119*, 5888.

(42) Yokonuma, N.; Furukawa, Y.; Tasumi, M.; Kuroda, M.; Nakayama, J. *Chem. Phys. Lett.* **1996**, *255*, 431.

(43) Wintgens, V.; Valat, P.; Garnier, F. *J. Phys. Chem.* **1994**, *98*, 228.

(44) Fichou, D.; Horowitz, G.; Xu, B.; Garnier, F. *Synth. Met.* **1990**, *39*, 243.

(45) Zinger, B.; Mann, K. R.; Hill, M. G.; Miller, L. L. *Chem. Mater.* **1992**, *4*, 1113.

(46) Hill, M. G.; Penneau, J. F.; Zinger, B.; Mann, K. R.; Miller, L. L. *Chem. Mater.* **1992**, *4*, 1106.

(47) Helbig, M.; Hein, J.; Rentsch, S.; Burger, H.; Hobert, H. *Chem. Phys.* **1998**, *227*, 111.

(48) Evans, C. H.; Scaiano, J. C. *J. Am. Chem. Soc.* **1990**, *112*, 2694.

(49) Kankare, J.; Lukkari, J.; Pasanen, P.; Sillanpaa, R.; Laine, H.; Harmaa, K.; Visy, C. *Macromolecules* **1994**, *27*, 4327.

(50) Ma, J.; Li, S.; Jiang, Y. *Macromolecules* **2002**, *35*, 1109.

(51) Della Sala, F.; Heinze, H. H.; Gorling, A. *Chem. Phys. Lett.* **2001**, *339*, 343.

(52) Hsu, C.-P.; Hirata, S.; Head-Gordon, M. *J. Phys. Chem. A* **2001**, *105*, 451.

(53) Pou-Amerigo, R.; Viruela, P. M.; Viruela, R.; Rubio, M.; Orti, E. *Chem. Phys. Lett.* **2002**, *352*, 491.

(54) Clarke, T. M.; Gordon, K. C.; Officer, D. L.; Grant, D. K. *J. Chem. Phys.* **2006**, *124*, 164501.

(55) Clarke, T. M.; Gordon, K. C.; Officer, D. L.; Grant, D. K. *J. Phys. Chem. A* **2005**, *109*, 1961.

(56) Clarke, T. M.; Gordon, K. C.; Officer, D. L.; Hall, S. B.; Collis, G. E.; Burrell, A. K. *J. Phys. Chem. A* **2003**, *107*, 11505.

(57) Iwao, M.; Lee, M. L.; Castle, R. N. *J. Heterocycl. Chem.* **1980**, *17*, 1259.

(58) Noviandri, I.; Brown, K. N.; Fleming, D. S.; Gulyas, P. T.; Lay, P. A.; Masters, A. F.; Phillips, L. *J. Phys. Chem. B* **1999**, *103*, 6713.

(59) Frisch, M. J.; G. W. T.; Schlegel, H. B.; Scuseria, G. E.; Robb, M. A.; Cheeseman, J. R.; Montgomery, J. A., Jr.; Vreven, T.; Kudin, K. N.; Burant, J. C.; Millam, J. M.; Iyengar, S. S.; Tomasi, J.; Barone, V.; Mennucci, B.; Cossi, M.; Scalmani, G.; Rega, N.; Petersson, G. A.; H. N.; Hada, M.; Ehara, M.; Toyota, K.; Fukuda, R.; Hasegawa, J.; Ishida, M.; Nakajima, T.; Honda, Y.; Kitao, O.; Nakai, H.; Klene, M.; Li, X.; Knox, J. E.; Hratchian, H. P.; Cross, J. B.; Adamo, C.; Jaramillo, J.; Gomperts, R.; Stratmann, R. E.; Yazyev, O.; Austin, A. J.; Cammi, R.; Pomelli, C.; Ochterski, J. W.; Ayala, P. Y.; K. Morokuma, G.; Voth, A.; Salvador, P.; Dannenberg, J. J.; Zakrzewski, V. G.; Dapprich, S.; Daniels, A. D.; Strain, M. C.; Farkas, O.; Malick, D. K.; Rabuck, A. D.; Raghavachari, K.; Foresman, J. B.; Ortiz, J. V.; Cui, Q.; Baboul, A. G.; Clifford, S.; Cioslowski, J.; Stefanov, B. B.; Liu, G.; Liashenko, A.; Piskorz, P.; Komaromi, I.; Martin, R. L.; Fox, D. J.; Keith, T.; Al-Laham, M. A.; Peng, C. Y.; Nanayakkara, A.; Challacombe, M.; Gill, P. M. W.; Johnson, B.; W. C.; Wong, M. W.; Gonzalez, C.; Pople, J. A. *Gaussian 03*; Gaussian, Inc.: Pittsburgh, PA, 2003.

(60) Scott, A. P.; Radom, L. *J. Phys. Chem.* **1996**, *100*, 16502.

(61) Bonfantini, E. E.; Officer, D. L. *Chem. Commun.* **1994**, 1445.

(62) Collis, G. E.; Burrell, A. K.; Officer, D. L. *Tet. Lett.* **2001**, *42*, 8733.

(63) Wagner, P.; Officer, D. L.; Kubicki, M. Manuscript in preparation.

(64) Silverstein, R. M.; Bassler, G. B.; Morrill, T. C. *Spectrometric Identification of Organic Compounds*, 5th ed.; John Wiley & Sons, Inc.: Singapore, 1991.

(65) Andrews, L.; Friedman, R. S.; Kelsall, B. J. *J. Phys. Chem.* **1985**, *89*, 4016.

(66) Szczepanski, J.; Vala, M.; Talbi, D.; Parisel, O.; Ellinger, Y. *J. Chem. Phys.* **1993**, *98*, 4494.

(67) Masnovi, J. M.; Kochi, J. K. *J. Phys. Chem.* **1987**, *91*, 1878.

(68) Leong, B.; Pope, M.; Steigman, J. *J. Phys. Chem.* **1988**, *92*, 2506.

(69) Khan, M. N.; Palivan, C.; Barbosa, F.; Amaudrut, J.; Gescheidt, G. *J. Chem. Soc., Perkin Trans.* **2001**, *2*, 1522.

(70) Howarth, O. W.; Fraenkel, G. K. *J. Am. Chem. Soc.* **1966**, *88*, 4514.

(71) Visser, R. J.; Weisenborn, P. C. M.; Van Kan, P. J. M.; Huizer, B. H.; Varma, C. A. G. O.; Warman, J. M.; De Haas, M. P. *J. Chem. Soc., Faraday Trans. 2* **1985**, *81*, 689.

(72) Audebert, P.; Catel, J. M.; Le Coustumer, G.; Duchenet, V.; Hapiot, P. *J. Phys. Chem. B* **1998**, *102*, 8661.

(73) Barth, M.; Guillerez, S.; Bidan, G.; Bras, G.; Lapkowski, M. *Electrochim. Acta* **2000**, *45*, 4409.

(74) Clarke, T. M.; Gordon, K. C.; Chan, W. S.; Phillips, D. L.; Wagner, P.; Officer, D. L. *Chem. Phys. Chem.* **2006**, *7*, 1276.

(75) Bredas, J. L.; Calbert, J. P.; Da Silva Filho, D. A.; Cornil, J. *Proc. Natl. Acad. Sci. U.S.A.* **2002**, *99*, 5804.